

Modelling of partially coherent radiation based on the coherent mode decomposition

Andrej Singer^{1,*} and Ivan A. Vartanyants^{1,2,†}

¹*Deutsches Elektronen-Synchrotron DESY,*

Notkestr. 85, D-22607 Hamburg, Germany

²*National Research Nuclear University, "MEPhI", 115409 Moscow, Russia*

Abstract

We present a method for the propagation of partially coherent radiation using coherent mode decomposition and wavefront propagation. The radiation field is decomposed into a sum of independent coherent modes. Each mode is then propagated separately using conventional wavefront propagation techniques. The summation of these modes in the plane of observation gives the coherence properties of the propagated radiation. As an example, we analyze propagation of partially coherent radiation transmitted through a single circular aperture.

PACS numbers: 42.25.Kb, 42.25.Bs, 41.60.Cr

INTRODUCTION

With the construction of the third generation synchrotron sources (see for example [1]) partially coherent radiation in the x-ray range has become available. The advent of the free-electron lasers [2, 3] has tremendously increased the amount of coherent flux, that can be used by experimentalists. Techniques like coherent x-ray diffractive imaging (CXDI) [4–6] explicitly utilize the high coherent flux and promise new insights in structural biology, condensed matter physics, magnetism and other correlated systems [7].

Careful planing of the coherence-based experiments is required, which means that the knowledge of the beam properties at the experimental station is in high demand. Although many computational methods have been developed to calculate the beam profile at the sample position, most of them do not provide the coherence properties of the beam in the plane of observation. In addition, the majority of these calculations are based on the ray tracing, or the wave propagation approach and are valid only in the limit of incoherent or fully coherent radiation, respectively. At the same time, partially coherent radiation that is mostly available nowadays at the 3rd generation synchrotron sources and free electron lasers is not covered by these methods.

Here, we present a general approach, which can be applied to partially coherent wavefields, and which is capable of calculating both the intensity profile of the beam as well as the transverse coherence properties of the radiation at any position in the beamline. It is based on the results of statistical optics, where the radiation field is described in terms of correlation functions. In this work we represent the correlation function of the radiation field as a sum of coherent modes [8]. Each mode is propagated separately through the beamline optics using a wave propagation technique. At the sample position the correlation function is given as a sum of the propagated modes. The intensity profile and the transverse coherence properties of the radiation can be readily extracted from this correlation function. A similar approach was used in the frame of geometrical optics [9] and for advanced phase retrieval methods in coherent imaging [10].

We applied this technique to calculate the radiation properties of a Gaussian Schell-model source. As an example, source parameters of the free electron laser in Hamburg (FLASH) were considered and propagation of the partially coherent radiation through a pinhole was analyzed.

METHODS

Definitions

In the theory of partial coherence the mutual coherence function, $\Gamma(\mathbf{r}_1, \mathbf{r}_2; \tau)$, plays the dominant role. It describes the correlation between two complex scalar values of the electric field, $E(\mathbf{r}; t)$, at different points $\mathbf{r}_1, \mathbf{r}_2$ and at different times t and $t + \tau$ [8, 11]

$$\Gamma(\mathbf{r}_1, \mathbf{r}_2; \tau) = \langle E(\mathbf{r}_1; t)^* E(\mathbf{r}_2; t + \tau) \rangle_T, \quad (1)$$

where the brackets $\langle \dots \rangle_T$ denote the time average. It is assumed that the averaging is performed over times T that are much longer than the fluctuation time of the field [12]. When we consider the propagation of the correlation functions in space, it is convenient to introduce the cross spectral density function, $W(\mathbf{r}_1, \mathbf{r}_2; \omega)$, as the Fourier transform of the mutual coherence function [8]

$$W(\mathbf{r}_1, \mathbf{r}_2; \omega) = \int \Gamma(\mathbf{r}_1, \mathbf{r}_2; \tau) e^{i\omega\tau} d\tau, \quad (2)$$

where ω is the angular frequency of the radiation. By definition, when the two points \mathbf{r}_1 and \mathbf{r}_2 coincide, the cross spectral density represents the spectral density [13] of the radiation field, $I(\mathbf{r}; \omega) = W(\mathbf{r}, \mathbf{r}; \omega)$. The normalized cross spectral density is known as the spectral degree of coherence

$$\mu_{12}(\omega) = \frac{W(\mathbf{r}_1, \mathbf{r}_2; \omega)}{\sqrt{I(\mathbf{r}_1; \omega)I(\mathbf{r}_2; \omega)}}, \quad 0 \leq |\mu_{12}| \leq 1. \quad (3)$$

The modulus of the spectral degree of coherence is often measured in interference experiments as the contrast of the interference fringes. To characterize the transverse coherence properties of the wavefield by a single number the normalized degree of coherence can be introduced [14]

$$\zeta(\omega) = \frac{\int |W(\mathbf{r}_1, \mathbf{r}_2; \omega)|^2 d\mathbf{r}_1 d\mathbf{r}_2}{(\int I(\mathbf{r}; \omega) d\mathbf{r})^2}. \quad (4)$$

Mode decomposition and propagation of the correlation function

It can be shown that under very general conditions the cross spectral density can be decomposed into a sum of statistically independent coherent modes [8]

$$W(\mathbf{r}_1, \mathbf{r}_2; \omega) = \sum_n \beta_n(\omega) E_n^*(\mathbf{r}_1; \omega) E_n(\mathbf{r}_2; \omega), \quad (5)$$

where $\beta_n(\omega)$ are the eigenvalues and $E_n(\mathbf{r}; \omega)$ are the eigenfunctions of the integral equation

$$\int W(\mathbf{r}_1, \mathbf{r}_2; \omega) E_n(\mathbf{r}_1; \omega) d\mathbf{r}_1 = \beta_n(\omega) E_n(\mathbf{r}_2; \omega). \quad (6)$$

In particular, the mode decomposition (5) can be applied to planar secondary sources [8], where the cross spectral density [15], $W(\mathbf{r}_1, \mathbf{r}_2) = W(\mathbf{u}_1, \mathbf{u}_2; z_0)$, of the radiation field is given in the source plane with the transverse coordinates $\mathbf{u} = (x, y)$. The coordinate z is defined along the optical axis and the position of the source is at $z_0 = 0$.

The mode decomposition is convenient in the analysis of the propagation of partially coherent radiation, when only a small number of modes is required to describe the cross spectral density. The coherent modes can be propagated separately along the optical axis and the cross spectral density function, $W(\mathbf{u}_1, \mathbf{u}_2; z)$, can be calculated at any position z along the optical axis via eq. (5) replacing the modes $E_n(\mathbf{u}, z_0)$ by the propagated modes $E_n(\mathbf{u}, z)$. The eigenvalues, β_n , remain unchanged during the propagation.

The propagation of the field for each mode over a distance z along the optical axis can be performed by a wave propagation technique. In the case of free space propagation this can be done utilizing the Huygens-Fresnel principle [16]

$$E_n(\mathbf{u}, z) = \int P_z(\mathbf{u}, \mathbf{u}') E_n(\mathbf{u}', z_0) d\mathbf{u}', \quad (7)$$

where $E_n(\mathbf{u}', z_0)$ is the wavefield of the mode in the source plane and $E_n(\mathbf{u}, z)$ is the propagated mode at position z . The propagator $P_z(\mathbf{u}, \mathbf{u}')$ is given by

$$P_z(\mathbf{u}, \mathbf{u}') = \frac{k}{2\pi i} \frac{e^{ikr}}{r} \chi(\theta).$$

where $k = \omega/c$ is the wavevector, r is the distance between the points (\mathbf{u}', z_0) and (\mathbf{u}, z) , θ is the angle between the line joining (\mathbf{u}', z_0) to (\mathbf{u}, z) and the optical axis, and $\chi(\theta)$ is the obliquity factor with $\chi(0) = 1$ and $0 \leq \chi(\theta) \leq 1$. In the paraxial approximation, when small angles θ are considered, the propagator reduces to

$$P_z(\mathbf{u} - \mathbf{u}') = \frac{k}{2\pi i z} \exp \left[\frac{ik}{2z} (\mathbf{u} - \mathbf{u}')^2 \right].$$

In general, the propagation of the partially coherent radiation through an arbitrary arrangement of the optical elements in a beamline can be performed in the following steps

1. Decomposition of the cross spectral density, $W(\mathbf{u}_1, \mathbf{u}_2; z_0)$, of the source into coherent modes $E_n(\mathbf{u}, z_0)$ according to eq. (5).

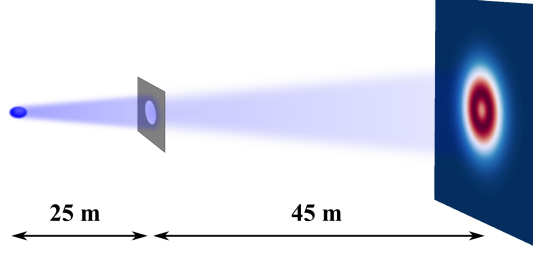


FIG. 1: Partially coherent radiation is generated at the source. The circular aperture is positioned 25 m downstream from the source. The coherence properties of the radiation are analyzed 45 m downstream from the aperture.

2. Propagation of all modes $E_n(\mathbf{u}, z_0)$ from the source plane through the optical elements to the observation plane using a wave propagation technique. For example, equation (7) can be used to propagate all modes from the source to the first optical element at the position z . For thin optical elements the transmitted modes are given by $E^{out}(\mathbf{u}, z) = T(\mathbf{u})E(\mathbf{u}, z)$, where $T(\mathbf{u})$ is the transmission function. At the next step the transmitted modes are propagated to the next optical element using eq. (7).
3. Finally, after performing the previous step for all optical elements present in the beam-line each mode is calculated in the plane of observation, and the cross spectral density, $W(\mathbf{u}_1, \mathbf{u}_2; z)$, is determined by eq. (5).

Gaussian Schell-model

A useful model to describe the radiation properties of partially coherent sources is the Gaussian Schell-model [8]. This model has been applied for the analysis of the radiation field generated by optical lasers [17], third generation synchrotron sources [14] and x-ray free-electron lasers [18–20]. In this model the cross spectral density in the source plane, $W(\mathbf{u}_1, \mathbf{u}_2; z_0)$, is given by

$$W(\mathbf{u}_1, \mathbf{u}_2; z_0) = \exp\left(-\frac{x_1^2 + x_2^2}{2\sigma_x^2} - \frac{y_1^2 + y_2^2}{2\sigma_y^2}\right) \exp\left(-\frac{(x_2 - x_1)^2}{2\xi_x^2} - \frac{(y_2 - y_1)^2}{2\xi_y^2}\right), \quad (8)$$

where σ_x , σ_y is the source size and ξ_x , ξ_y is the transverse coherence length of the source in the horizontal (x) and vertical (y) direction, respectively. Due to the symmetry of the Gaussian Schell-model the total cross spectral density at the source factorizes into the horizontal

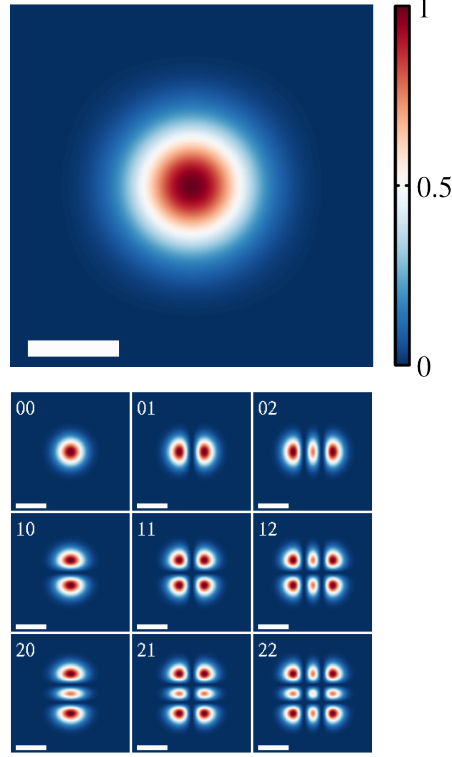


FIG. 2: (top) The total intensity distribution at the source position. (bottom) The intensity distribution of the nine lowest modes at the source position. The length of the white scale bar is $150 \mu\text{m}$.

and vertical components

$$W(\mathbf{u}_1, \mathbf{u}_2; z_0) = W(x_1, x_2; z_0) \cdot W(y_1, y_2; z_0). \quad (9)$$

The modes E_n and their corresponding contributions β_n can be found for each direction separately

$$W(x_1, x_2; z_0) = \sum_n \beta_n^x E_n^*(x_1; z_0) E_n(x_2; z_0),$$

and a similar expression is valid for the y direction. The analytical solution of the integral equation (6) for the Gaussian Schell-model in each direction is known in the form of the Gaussian Hermite-modes. The eigenvalues in this model are described by a power law [8]. The total cross spectral density is given by

$$W(\mathbf{u}_1, \mathbf{u}_2; z_0) = \sum_{n,m} \beta_{nm} E_{nm}^*(\mathbf{u}_1; z_0) E_{nm}(\mathbf{u}_2; z_0), \quad (10)$$

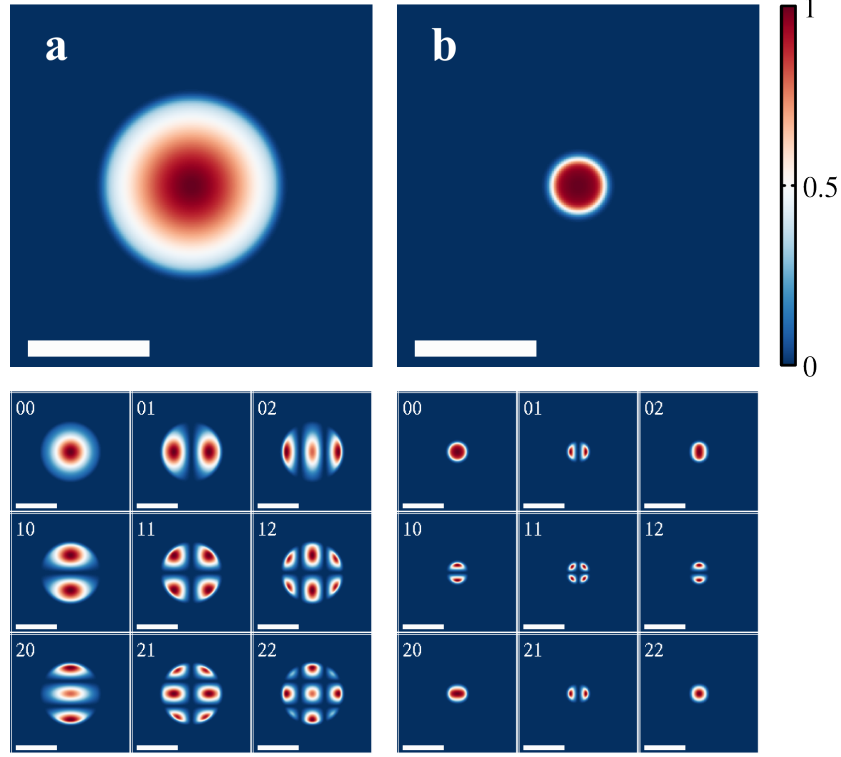


FIG. 3: (top) The total intensity distribution behind a circular aperture with (a) 3mm and (b) 1 mm diameter. (bottom) The intensity of the lowest nine modes behind the aperture. The length of the scale bar is 2 mm.

where $E_{nm}(\mathbf{u}; z_0) = E_n(x; z_0) \cdot E_m(y; z_0)$ are the well known laser resonator TEM_{nm} modes [21] and $\beta_{nm} = \beta_n^x \beta_m^y$. The total radiated intensity can be calculated by

$$I(\mathbf{u}; z_0) = W(\mathbf{u}, \mathbf{u}; z_0) = \sum_{n,m} \beta_{nm} |E_{nm}(\mathbf{u}; z_0)|^2. \quad (11)$$

We want to note here that our approach is not limited to the Gaussian Schell-model. If the cross spectral density of the field, $W(\mathbf{u}_1, \mathbf{u}_2; z_0)$, at the source is known, the corresponding modes E_n and their contributions β_n can be calculated from the integral equation (6) (see for example Ref. [22]).

PROPAGATION OF PARTIALLY COHERENT RADIATION THROUGH A CIRCULAR APERTURE

We simulated the propagation of the partially coherent radiation generated by a Gaussian Schell-model source through a circular aperture (see Figure 1). As source parameters we

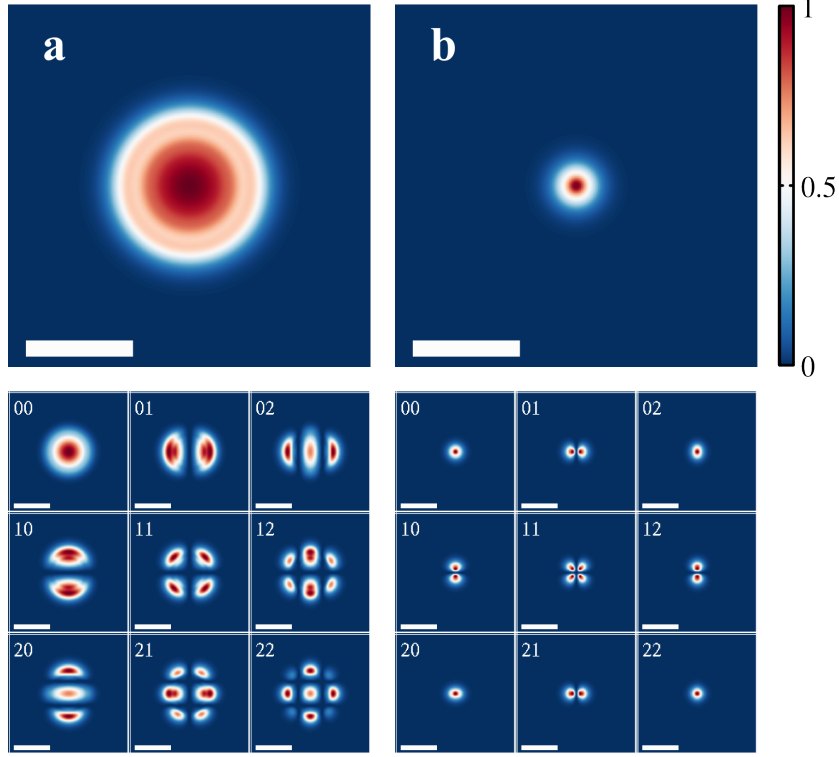


FIG. 4: (top) The total intensity distribution in the plane of observation calculated for a circular aperture, (a) 3mm and (b) 1 mm in diameter. (bottom) The intensity distribution of the lowest nine modes in the plane of observation. The length of the scale bar is 5 mm.

used values reported for FLASH [2] operating at a wavelength of 13.5 nm: the full width at half maximum (FWHM) source size is $160\mu\text{m}$ and the FWHM divergence of the beam is $90\mu\text{rad}$. In the frame of the Gaussian Schell-model (see eq. (8)) these values correspond to $\sigma_x = \sigma_y = 68\mu\text{m}$ and $\xi_x = \xi_y = 62\mu\text{m}$ [18]. For these parameters the contribution of each mode at the source position is given by the power law $\beta_{nm} = 0.41^{n+m}$. Modes with a contribution of less than 1 % were neglected in our simulations. In total, 21 modes with $n + m \leq 5$, where $n = 0, 1, \dots, 5$, $m = 0, 1, \dots, 5$, were used in the calculations presented here. The intensity distribution of the total field and the nine lowest modes at the source position are shown in Figure 2.

We considered the following geometry in our simulations: the pinhole is positioned 25 m downstream from the source and the radiation properties are analyzed 70 m downstream from the source (see Figure 1). Such an arrangement is typical for experiments performed in the unfocused beam at FLASH. We applied the general scheme of propagation of partially

coherent radiation described earlier for this experimental geometry. The propagation in the free space was performed using equation (7) with the propagator in the paraxial approximation. Different pinholes with the diameter from 5 mm to 1 mm were analyzed. The pinhole transmission function, $T(\mathbf{u})$, was defined as

$$T(\mathbf{u}) = \begin{cases} 1 & \text{for } |\mathbf{u}| < d/2 \\ 0 & \text{elsewhere} \end{cases},$$

where d is the diameter of the pinhole. It was convolved with a 200 μm wide (FWHM) Gaussian function to account for imperfections of the pinhole edges. The intensity distribution of the total beam and the lowest modes behind 3 mm and 1 mm pinholes are presented in Figure 3. Figure 4 shows the same in the plane of observation.

One readily sees in Figure 3 (a) that in the case of the 3 mm pinhole the first modes, which dominate the radiation field, are just slightly affected by the aperture. The 1 mm pinhole, however, substantially cuts all modes, including the dominant ones (see Figure 3 (b)). The intensity distribution of each mode in the plane of observation is similar to the intensity distribution leaving the pinhole. Additional intensity modulations due to the scattering on the edges of the aperture are observed in Figure 4 (a). This can be attributed to the Fresnel diffraction effects, which are stronger for sharper pinhole boundaries. The Fresnel number, $d^2/(\lambda L)$, where λ is the wavelength of the radiation and L is the distance from the pinhole to the detector, is 15 for the 3 mm pinhole and 1.6 for the 1 mm pinhole in this experimental geometry. We want to note here that due to Fresnel diffraction, small variations in the propagation distances might change these intensity modulations significantly.

Finally, the cross spectral density, $W(\mathbf{u}_1, \mathbf{u}_2; z)$, was determined in the plane of observation. We present here results for the horizontal direction

$$W(x_1, x_2; z) = \sum_{nm} \beta_{nm} E_{nm}^*(x_1, y_1 = 0; z) E_{nm}(x_2, y_2 = 0; z). \quad (12)$$

Due to the symmetry of our scattering geometry, the same result is obtained in the vertical direction. The modulus of the cross spectral density, $|W(x_1, x_2; z)|$, as a function of the transverse positions, x_1 and x_2 , is shown in Figure 5 (a-d) for different apertures. The modulus of the spectral degree of coherence $|\mu(\Delta x)| = |\mu(-\Delta x/2, \Delta x/2)|$ as a function of the separation Δx for the same apertures is presented in Figure 5 (e-h) (red solid line). This calculation corresponds to the measurements of the contrast in a double pinhole experiment

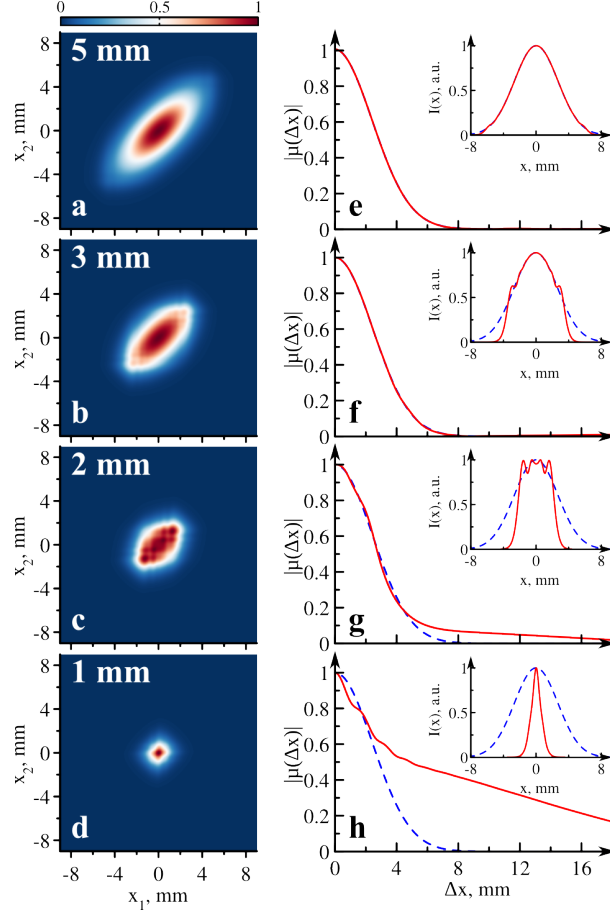


FIG. 5: Transverse coherence properties of the radiation in the observation plane. (a-d) The modulus of the cross spectral density $|W(x_1, x_2; z)|$. (e-h) The modulus of the spectral degree of coherence $|\mu(\Delta x)|$ as a function of the separation Δx . Simulations were performed with the pinhole diameters of (a,e) 5 mm, (b,f) 3 mm, (c,g) 2 mm, and (d,h) 1 mm. The insets in (e-h) show the intensity distribution $I(x)$ in the horizontal direction. Red solid lines show the simulations with the presence of the circular aperture. The blue dashed lines show the same functions obtained without the pinhole.

with varying pinhole separation Δx and the center of the double pinhole positioned at the optical axis of the beam. For comparison, the spectral degree of coherence, $|\mu(\Delta x)|$, for the same geometry and source parameters, but without the aperture is shown by the blue dashed line. The intensity profiles, $I(x)$, for the same aperture sizes are shown in the insets of Figure 5 (e-h).

As a result of our simulations, we notice that the 5 mm pinhole does not affect the transmitted radiation. The intensity profile $I(x)$ as well as the modulus of the spectral

degree of coherence $|\mu(\Delta x)|$ in the observation plane calculated with and without the pinhole are the same. For the smaller pinhole diameters of 3 mm and 2 mm the size of the beam decreases, but the modulus of the spectral degree of coherence is not significantly altered. Our simulations suggest, that in the present geometry down to the pinhole sizes of 2 mm no significant changes in the coherence properties of the beam in the observation plane are expected. Only for the smallest pinhole size of 1 mm the values of $|\mu(\Delta x)|$ are significantly enhanced at large separations (see Figure 5 (h)). In this case the spectral degree of coherence cannot be described by a single Gaussian function (compare to results of Ref. [23]). However, we should note here that these separations are much larger than the beam size and will be difficult to access in a real experiment.

We analyzed as well the normalized degree of coherence ζ (4) and the available photon flux P behind each pinhole (see Table 1). The transmitted photon flux was calculated by the equation $P = \int I_{out}(\mathbf{u})d\mathbf{u} / \int I_{in}(\mathbf{u})d\mathbf{u}$, where $I_{in}(\mathbf{u})$ and $I_{out}(\mathbf{u})$ are the intensity (see eq. (11)) incident on and behind the aperture. If no pinhole is present in the beamline, then obviously the photon flux $P = 100\%$ and the normalized degree of coherence has the value determined by the source parameters $\zeta = 18\%$. Results from the Table 1 show that the normalized degree of coherence, ζ , is significantly increased for the smaller pinholes. However, this happens at a loss of the transmitted photon flux P . It is interesting to note that the product $P \cdot \zeta$, which may be considered as the amount of the coherent photon flux, is about 20 % after transmission through the larger pinholes. It drops down to a value of only about 10 % for the 1 mm pinhole. In the latter case almost a fully coherent beam, $\zeta = 78\%$, is achieved with 10 % of the transmitted radiation.

TABLE I: The transmitted photon flux, P , and the normalized degree of coherence, ζ , behind the aperture. Four different pinhole diameters are analyzed.

no pinhole	$P = 100\% \quad \zeta = 18\%$
5 mm	$P = 97\% \quad \zeta = 19\%$
3 mm	$P = 69\% \quad \zeta = 29\%$
2 mm	$P = 39\% \quad \zeta = 46\%$
1 mm	$P = 10\% \quad \zeta = 78\%$

CONCLUSIONS

In conclusion, we have presented a computational method, that allows the calculation of the transverse coherence properties as well as the beam intensity profile of partially coherent radiation at any position in the beamline. Our approach can be easily implemented, since it is based on the wave front propagation, for which several powerful computational methods are already developed. The important extension to the conventional wave propagation methods is the consideration of all contributing modes.

We have applied this method to describe the propagation of partially coherent radiation through a circular aperture. Parameters typical for FLASH were used in the simulations. Our analysis shows, that the presence of the pinhole does not increase the transverse coherence length substantially, even if the beam is significantly cut by the aperture. At the same time, the normalized degree of coherence is significantly increased for smaller pinholes at the expense of the available photon flux. A straightforward extension to our approach would be its application to a beamline with a number of optical elements. Our simulations suggest that a careful calculation is important to have a realistic picture of the beam properties in the observation plane for a concrete realization of the optics in the beamline. An interesting question, for example, would be how imperfections of the optical elements affect the transverse coherence length of the radiation.

This approach can be effectively used to describe the radiation at free electron lasers, which is predominantly coherent and contains a small number of statistically independent modes. It can be also applied to third generation synchrotron sources, which are highly coherent in the vertical direction and less coherent in the horizontal direction [14]. However, in this case a significantly larger number of modes has to be taken into account.

We would like to thank Edgar Weckert for his interest and support of this work and Ulf Lorenz for his careful reading of the manuscript. Part of this work was supported by BMBF Proposal 05K10CHG "Coherent Diffraction Imaging and Scattering of Ultrashort Coherent Pulses with Matter" in the framework of the German-Russian collaboration "Development and Use of Accelerator-Based Photon Sources".

-
- * email: andrej.singer@desy.de
- † email: ivan.vartanyants@desy.de
- [1] See for example <http://petra3.desy.de/>
 - [2] W. Ackermann *et al.*, "Operation of a free-electron laser from the extreme ultraviolet to the water window," Nat. Photon., **1** 336 (2007).
 - [3] P. Emma *et al.*, "First lasing and operation of an angstrom-wavelength free-electron laser," Nat. Photon., **4**, 641 (2010).
 - [4] J. Miao, *et al.* "Extending the methodology of X-ray crystallography to allow imaging of micrometre-sized non-crystalline specimens," Nature (London) **400**, 342 (1999).
 - [5] M. A. Pfeifer, *et al.* "Three-dimensional mapping of a deformation field inside a nanocrystal," Nature (London) **442**, 63 (2006)
 - [6] H. N. Chapman *et al.*, "Femtosecond diffractive imaging with a soft-X-ray free-electron laser," Nature Physics, **2**, 839 (2006).
 - [7] I. A. Vartanyants *et al.* "Coherent X-ray scattering and lensless imaging at the European XFEL Facility", J. Synchrotron Rad. **14**, 453 (2007).
 - [8] L. Mandel and E. Wolf, *Optical Coherence and Quantum Optics* (Cambridge University Press, 1995)
 - [9] A. M. Zysk, P. S. Carney, and J. C. Schotland "Eikonal Method for Calculation of Coherence Functions," Phys. Rev. Lett. **95**, 043904 (2005)
 - [10] L. W. Whitehead *et al.* "Diffractive Imaging Using Partially Coherent X Rays," Phys. Rev. Lett. **103**, 243902 (2009)
 - [11] J. W. Goodman, *Statistical Optics* (Wiley, New York, 2000)
 - [12] For pulsed sources like free-electron lasers this assumption means that the pulse duration is much longer than the temporal coherence time.
 - [13] For the narrow-bandwidth light, that will be considered in the following, it corresponds to the intensity distribution at the average frequency $\bar{\omega}$.
 - [14] I. A. Vartanyants and A. Singer, "Coherence properties of hard x-ray synchrotron sources and x-ray free-electron lasers," New J. Phys. **12**, 035004 (2010)
 - [15] In all equations below, we omit ω for brevity.

- [16] M. Born and E. Wolf, *Principles of optics* (Cambridge University Press, 1999)
- [17] F. Gori, "Collett-Wolf Sources and Multimode Lasers," *Opt. Commun.* **34**, 301 (1980)
- [18] A. Singer *et al.*, "Transverse-Coherence Properties of the Free-Electron-Laser FLASH at DESY," *Phys. Rev. Lett.* **101**, 254801 (2008).
- [19] S. Roling *et al.*, "Temporal and spatial coherence properties of Free Electron Laser pulses in the XUV regime," *Phys. Rev. ST Accel. Beams* (accepted)
- [20] I. Vartanians *et al.* "Coherence Properties of Individual Femtosecond Pulses of an X-ray Free-Electron Laser," *Phys. Rev. Lett.* (submitted)
- [21] F. Gori, "Mode propagation of the field generated by Collett-Wolf Schell-model sources," *Opt. Commun.* **46**, 149 (1983)
- [22] S. Flewett *et al.* "Extracting coherent modes from partially coherent wavefields," *Optics Letters* **34**, 2198 (2009)
- [23] J. J. A. Lin *et al.*, "Measurement of the Spatial Coherence Function of Undulator Radiation using a Phase Mask," *Phys. Rev. Lett.* **90**, 074801 (2003)